# UCSF

**UC San Francisco Previously Published Works**

## Title

Identifying specific prefrontal neurons that contribute to autism-associated abnormalities in physiology and social behavior.

## Permalink

https://escholarship.org/uc/item/88x805pt

## Journal

Molecular psychiatry, 23(10)

## ISSN

1359-4184

## Authors

Brumback, AC
Ellwood, IT
Kjaerby, C
et al.

## Publication Date

2018-10-01

## DOI

10.1038/mp.2017.213

Peer reviewed

# Identifying specific prefrontal neurons that contribute to autism-associated abnormalities in physiology and social behavior

**Audrey C. Brumback, MD, PhD**[1,2,4,*], **Ian Elwood, PhD**[2,*], **Celia Kjaerby, PhD**[2,*], **Jillian Iafrati, PhD**[2], **Sarah Robinson, BS**[2], **Anthony Lee, BS**[2], **Tosha Patel, MS**[2], **Suraj Nagaraj, BS**[2], **Felicia Davatolhagh, BS**[2], and **Vikaas S. Sohal, MD, PhD**[3]

[1]Department of Neurology, Weill Institute for Neurosciences, Kavli Institute for Fundamental Neuroscience, University of California, San Francisco, San Francisco, CA, USA.

[2]Department of Psychiatry, Weill Institute for Neurosciences, Kavli Institute for Fundamental Neuroscience, University of California, San Francisco, San Francisco, CA, USA.

[3]Department of Psychiatry, Weill Institute for Neurosciences, Kavli Institute for Fundamental Neuroscience, University of California, San Francisco, San Francisco, CA, USA.

[4]Current address: Departments of Neurology and Pediatrics, Dell Medical School, and Center for Learning and Memory at The University of Texas at Austin

## Abstract

Functional imaging and gene expression studies both implicate the medial prefrontal cortex (mPFC), particularly deep layer projection neurons, as a potential locus for autism pathology. Here, we explored how specific deep-layer prefrontal neurons contribute to abnormal physiology and behavior in mouse models of autism. First, we find that across three etiologically distinct models – *in utero* valproic acid (VPA) exposure, *CNTNAP2* knockout, and *FMR1* knockout – layer 5 subcortically-projecting (SC) neurons consistently exhibit reduced input resistance and action potential firing. To explore how altered SC neuron physiology might impact behavior, we took advantage of the fact that in deep layers of the mPFC, dopamine D2 receptors (D2Rs) are mainly expressed by SC neurons, and used D2-Cre mice to label D2R+ neurons for calcium imaging or optogenetics. We found that social exploration preferentially recruits mPFC D2R+ cells, but that this recruitment is attenuated in VPA-exposed mice. Stimulating mPFC D2R+ neurons disrupts normal social interaction. Conversely inhibiting these cells enhances social behavior in VPA-exposed mice. Importantly, this effect was not reproduced by nonspecifically

Corresponding author: Vikaas S. Sohal, 675 Nelson Rising Lane, San Francisco, CA 94143-0444, Tel: (415) 502-7377, vikaas.sohal@ucsf.edu.
*These authors contributed equally.

inhibiting mPFC neurons in VPA-exposed mice, or by inhibiting D2R+ neurons in wildtype mice. These findings suggest that multiple forms of autism may alter the physiology of specific deep-layer prefrontal neurons which project to subcortical targets. Furthermore, a highly overlapping population – prefrontal D2R+ neurons – plays an important role in both normal and abnormal social behavior, such that targeting these cells can elicit potentially therapeutic effects.

## INTRODUCTION

Autism spectrum disorder causes lifelong disability in millions of people [1]. Despite its high prevalence, there is no cure and treatments for core symptoms, such as social deficits, have been elusive. Although many genes have now been implicated in autism, specific cellular abnormalities that link genes with behavior remain obscure. Functional imaging studies reveal that the prefrontal cortex (PFC) is heavily involved in social cognition, specifically in analyzing the emotions and intentions of others [2,3]. The medial PFC (mPFC) is particularly important: lesions cause loss of social skills [4] and impair emotional learning [5]. In rodents, acute optogenetic manipulation of the excitatory/inhibitory balance within mPFC disrupts normal social exploration [6]. In humans, genes strongly linked to autism are convergently co-expressed within layers 5 and 6 (L5/6) projection neurons in the PFC during midfetal development [7], and in human autism, functional imaging studies reveal abnormally decreased activation of the mPFC during social tasks [3,8,9].

Human studies demonstrate that autism includes abnormal structural and functional connectivity between the PFC and subcortical structures such as the thalamus [10,11], but it is not known to what extent these defects might reflect abnormal electrical signaling within specific neurons that link the PFC and thalamus. mPFC neurons which project to the mediodorsal (MD) thalamus reside in L5/6. Previous studies have found changes in neuronal excitability and synaptic connectivity in L5 neurons in the mPFC of autism models [12,13]; however, it is not clear whether these represent nonspecific changes, or alternatively, whether they might differentially affect specific subpopulations of L5 neurons [14,15]. Work from our lab [16,17] and others [18,19] has shown that in the mPFC, L5 pyramidal neurons can be divided into distinct subpopulations that project to different targets. We hypothesized that 1) these various subtypes of prefrontal projection neurons might be differentially affected in autism, disrupting specific prefrontal circuit interactions; 2) if disruptions in specific circuits play important roles in core aspects of autism, then associated changes in the physiology of specific neuronal subtypes should be conserved across multiple etiologies of autism; 3) if neuronal subtypes which play particularly important roles in social behavior are abnormal in autism, then manipulations which target these subtypes may effectively ameliorate autism-associated behavioral abnormalities.

Human autism is associated with a diverse array of environmental and genetic etiologies that have been modeled with good construct validity in rodents. For instance, in humans, prenatal exposure to valproic acid (VPA), but not other anticonvulsants, is associated with a markedly increased prevalence of autism [20,21]. The offspring of pregnant rodents exposed to VPA at a specific time point (around the time of neural tube closure, embryonic day ~10.5) similarly exhibit the core deficits of autism [22]. In humans, mutations in the genes contactin-associated

protein-like 2 (*CNTNAP2*), which encodes a cell adhesion molecule [23], and fragile X mental retardation 1 (*FMR1*), which encodes an mRNA binding protein) [24] are both associated with autism. Mice lacking both copies of *CNTNAP2* show autistic features: juveniles spend less time interacting with each other and pups emit fewer isolation-induced ultrasonic vocalizations [25]. *FMR1* knockout (KO) mice [26] display social anxiety, deficits in communication, repetitive behaviors, and hyperactivity [27].

This study consists of two parts. First, to identify specific prefrontal circuits that may play important roles in autism, we looked for physiological abnormalities that were specific for particular neuronal subtypes and conserved across multiple autism models. For this, we analyzed the electrophysiological properties of prefrontal L5 projection neurons across the three autism models described above. In every case, we found a reduction in the excitability and input resistance of subcortically projecting (SC) L5 pyramidal neurons. By contrast, changes in other subtypes of L5 neurons were more heterogeneous across models. Second, we sought to understand how SC neurons (or a similar neuronal population) might contribute to normal, pathological, and potentially therapeutic aspects of social behavior. For this, we used D2-Cre mice to label a population of prefrontal neurons that is highly enriched for SC neurons. Then we examined how this population is recruited during normal and abnormal social behavior, and how optogenetically manipulating this neuronal subtype affects normal social behavior and social deficits associated with autism.

## METHODS

### Animals

All experiments were conducted in accordance with procedures established by the Administrative Panels on Laboratory Animal Care at the University of California, San Francisco. Mice were fed *ad libitum* and reared in normal lighting conditions (12h/12h light/dark cycle). We used the following mouse lines: wild-type C57BL/6 (Simonsen), wild-type CD1 (Simonsen), FVB.129P2-Pde6b+ Tyrc-ch *Fmr1*^tm1Cgr^/J (Jackson), B6.129(Cg)-*Cntnap2*^tm1Pele^/J (Jackson), *Drd2-Cre* (line ER44; gensat.org). For Fragile X experiments, knockout animals were compared to wildtype littermates. For *CNTNAP2* experiments, knockout animals were compared to heterozygous littermates. We initially used a mating scheme of het het (to produce KO and WT littermate controls), but we had a very low yield of knockout mice. Given the lack of evidence that heterozygous *CNTNAP2* mutations are associated with autism [66], we used a het × KO breeding scheme to produce knockouts with heterozygous littermates as controls. For prenatal VPA exposure experiments, pregnant C57Bl/6 or CD1 mice received a single intraperitoneal (IP) dose of VPA (500 mg/kg) or saline vehicle at embryonic day (E) 10.5 [67]. Animals of both sexes were used for all experiments except for the experiments in Fragile X mice and their wildtype littermate controls which used only male mice.

### Fluorescent labeling of specific neuron populations

Mice were anesthetized with 2% isoflurane and mounted in a stereotactic frame. Craniotomies were made according to stereotaxic coordinates relative to Bregma. To label interneurons in the mPFC, we injected AAV encoding the *Dlxi1/2b* enhancer driving

mCherry into the ipsilateral mPFC as previously reported [17]. To selectively label subcortical projection (SC) or intratelencephalic (IT) neurons, we injected fluorescently-labeled latex microspheres (Retrobeads, Lumafluor) or fluorescently-labeled cholera toxin subunit B (CTB, Molecular Probes) into contralateral mPFC or ipsilateral MD thalamus. Coordinates for injection into contralateral mPFC were (in millimeters relative to Bregma): +1.7 anterior-posterior (AP), –0.3 mediolateral (ML), and –2.75 dorsoventral (DV). Coordinates for injection into ipsilateral MD thalamus were –1.7 AP, +0.3 ML, and –3.5 DV. We injected 500 nL at 150 nL/min for mPFC and 400 nL at 100 nL/min for MD thalamus. We waited 5 minutes after the end of the injection before slowly withdrawing the syringe. We waited 3–5 days following retrograde tracer injections before performing experiments. At the time of the experiments, we visually verified that retrograde tracer injections were targeted appropriately and that tracer was not present in nearby structures.

### Slice preparation

Mice 8–12 weeks old were deeply anesthetized with isoflurane and then decapitated. We prepared coronal slices 250 μm thick using ice-cold solution containing (in mM): 234 sucrose, 26 $NaHCO_3$, 11 glucose, 2.5 KCl, 10 $MgSO_4$, 1.25 $NaH_2PO_4$, and 0.5 $CaCl_2$. ACSF contained (in mM): 126 NaCl, 26 $NaHCO_3$, 14 glucose, 3 KCl, 2 $CaCl_2$, 2 $MgCl_2$, and 1 $NaH_2PO_4$. Slices were incubated in a warmed 50/50 mixture of ACSF and slicing solution at 30–32°C for 15 minutes and then at least one hour at room temperature before being used for recordings. During experiments, slices were perfused with ACSF and secured by placing a harp along the midline between the two hemispheres.

### Intracellular recordings

Somatic whole-cell patch recordings were obtained from retrogradely-labeled visually identified neurons in Layer 5 (L5) of infralimbic and prelimbic cortex using differential contrast video microscopy on an upright microscope (BX51WI; Olympus). Layer 2/3 was identified as the first tight band of cells deep to the pial surface. Layer 6 was identified as the tight band of cells superficial to the white matter. Layer 5 was defined as the relatively loosely packed cells between these two bands. Recordings were made using a Multiclamp 700A (Molecular Devices). Patch electrodes (tip resistance = 2–6 MΩ) were filled with the following (in mM): 118 K-gluconate, 10 KCl, 10 HEPES, 4 MgATP, 1 EGTA, and 0.3 $Na_3GTP$ (pH adjusted to 7.2 with KOH). Slices were continuously perfused with ACSF in an immersion chamber (Warner Instruments) with temperature maintained at 32.5±1°C. Series resistance was usually 10–20 MΩ, and experiments were discontinued above 30 MΩ or if action potentials failed to overshoot 0 mV.

We did not correct for liquid junction potential. We measured resting membrane potential in current clamp immediately following whole cell break in. Fast-spiking interneurons were distinguished from other interneuron subtypes based on narrow spike widths ( ≤1 ms), minimal adaptation during sustained firing, steep f/i slopes, and high peak firing rates (typically >100 Hz). We calculated input resistance from the steady-state voltage change measured in response to –50 pA current steps. We calculated membrane time constant as the time at which the membrane voltage decayed to 1/e of the initial value following –50 pA current steps. We calculated membrane capacitance as the membrane time constant divided

by input resistance. We estimated H current using the sum of the "sag" and "rebound" in response to –200 pA steps [16]. We quantified action potential firing during one second current steps from 0 to +400 pA in 50 pA intervals. We estimated action potential threshold as the point at which the third derivative of the membrane potential was maximal. Action potential half-width was estimated as the time (in msec) for the membrane potential to rise from the point halfway between the trough and peak to the peak and then fall to the point halfway between the peak and the trough.

### Histology

All viruses were obtained from the University of North Carolina (UNC) Vector Core. Mice were stereotactically injected with rAAV5-EF1alpha-DIO-eYFP-WPRE ("DIO-eYFP", UNC Vector Core) into the right mPFC, 1.5 μL total volume (750 nL at 150 nL/min at +0.30–0.32 / +1.70 / –2.25 plus 750 nL at 150 nL/min at +0.30–0.32 / +1.70 / –2.75). Coordinates are given as mm from Bregma (medial-lateral / anterior-posterior / dorsal-ventral). Fluorescently labeled CTB was injected into either the left mPFC (to label IT cells) or the right MD thalamus (to label SC cells). After 4 days, animals were deeply anesthetized with Euthasol and transcardially perfused with 4% paraformaldehyde. Brains were incubated in 4% PFA overnight and then sliced on a Leica vibratome into coronal sections 100 μm thick. Brain slices were mounted onto glass slides and imaged using a confocal microscope. We counted 100 cells per slice in prelimbic and infralimbic cortices in the area that had the maximum overlap between eYFP and the fluorescently labeled CTB.

### *In vivo* calcium imaging (fiber photometry)

To express genetically-encoded calcium indicators in *Drd1::Cre* and *Drd2::Cre* mice, 500 nL of AAV viral vector carrying GCaMP6s or GCaMP6f were infused unilaterally into the right mPFC (anterior-posterior (AP): +1.7 mm, mediolateral (ML): +0.3 mm) at four different depths at 125 nL/location (dorsoventral (DV): –2.0 mm; –2.25; –2.50 mm; –2.75 mm) at a rate of 100 nL/min. Fiber optic cannulas with zirconia sheaths (400 μm diameter, 0.48 NA; Doric Lenses, Quebec City, Canada) were implanted over the mPFC (AP: +1.7 mm; ML: +0.3 mm; DV: –2.5 mm). We waited 4–6 weeks before starting experiments.

The fiber photometry system was set up as previously reported [35]. The light from a 473 nm diode laser (Omicron) was chopped at 400 Hz and reflected off a dichroic (Semrock, FF495). It was then coupled into a 400 μm optical fiber (Thorlabs). The patchcord was attached to the implanted optical fibers, and GCaMP6 fluorescence was collected and focused through a bandpass filter (Semrock) onto a femtowatt silicon photoreceiver (Newport). The output was directed through a lock-in amplifier (Stanford Research Systems), digitized (LabJack), and recorded on a PC. Signals were collected at a sampling rate of 500 Hz.

To estimate the relative light intensity transmitted from the fiber tip centered in L5 to the neurons in Layer 2/3, we estimated the light intensity at a point 100 μm deep and 100 μm lateral to the fiber tip. We used the ScatterBrain matlab app [68]. Using this method, the relative light intensity was 0.0016 using the following parameters: Fiber radius: 100 μm;

Fiber numerical aperture: 0.22; Tissue scattering coefficient: 211 cm$^{-1}$; absorption coefficient: 0.6 cm$^{-1}$; anisotropy index: 0.86; refraction index: 1.36.

Data were aligned so the first sniff took place at time = 0 seconds. Peak $\Delta F/F_0$ was calculated as the maximum of the calcium response following the first sniff. We estimated the plateau as the mean $\Delta F/F_0$ at t = +60 seconds averaged over a 20 second window. Please note that in the photometry experiments presented in Fig. 3, the exploration epochs each lasted 3 minutes (in contrast to the photometry experiments presented in Fig. 4 and the optogenetics experiments presented in Fig. 5 in which exploration epochs lasted 5 minutes).

### *In vivo* optogenetic manipulations

To express halorhodopsin (eNpHR) or channelrhodopsin (ChR2) in D2R-expressing neurons, we stereotactically injected rAAV5-EF1α-DIO-eNpHR3.0-mCherry-WPRE or rAAV5-Ef1α-DIO-hChR2(H134R)-eYFP into the mPFC of *Drd2-Cre* mice. In control experiments in which no virus was expressed, we injected virus encoding Cre-dependent eNpHR into *Drd2-Cre* negative mice. To express halorhodopsin nonspecifically throughout the mPFC, we stereotactically injected rAAV5-hSyn-eNpHR3.0-mCherry-WPRE in mPFC of *Drd2-Cre* negative mice.

Virus encoding eNpHR was injected bilaterally at (in millimeters relative to Bregma) +1.7 AP, +0.32–0.35 and –0.32–0.35 ML, with 750 nL injected at –2.25 DV and 750 nL at –2.75 DV. In VPA mice, virus encoding ChR2 (1000 nL) was injected bilaterally at +1.7 AP, +0.32–0.35 and –0.32–0.35 ML, –2.25 DV. In non-VPA-exposed controls, 750 nL virus encoding ChR2 was injected into right mPFC (AP: +1.7 mm; ML: +0.3 mm; DV: –2.75 mm). In all cases, immediately following viral injections, fiber optic cannulas (Doric Lenses, Québec City) were implanted over the injected areas with the tips at –2.25 DV. Cannulas were silica multimode optical fibers with a flat tip, 0.22 numerical aperture, a 200 μm core, 240 μm outer diameter, with an outer layer of yellow polyamide buffer. Cannulas were affixed to the skull using Metabond dental cement (C&B). Following behavioral assays, we sacrificed mice and verified that virus expression and the fiber optic tips were localized within the mPFC.

To activate halorhodopsin (eNpHR), continuous green (532 nm) laser light was directed through the bilateral fiber optic at 10 mW total power (5 mW in each hemisphere). In VPA mice, channelrhodopsin (ChR2) was activated in bilateral mPFC using blue (473 nm) laser light in 5 ms square pulses at 10 Hz with total bilateral light power of 0.6 mW (0.3 mW in each hemisphere). In non-VPA-exposed controls, ChR2 was activated using 473 nm laser light in 5 ms square pulses at 10 Hz with a total unilateral light power of 2 mW.

### Behavioral assays

Audio and video were recorded for offline analysis. For optogenetic experiments, animals performed the task two times, one week apart. Animals were randomized to receive light on or off during the first week and the opposite during the second week. We made within-animal comparisons between the two trials. Animals were allowed to habituate to the fiber attached to their head for 10 minutes in their home cage prior to starting the trial. The laser was turned on and 60 seconds later a juvenile (3–4 week old) mouse of the same strain and

sex was introduced to the home cage. After 5 minutes, the juvenile was removed from the home cage and the laser turned off. After a 5 minute break, the laser was turned on again. After 60 seconds of light on, a novel object (typically a plastic test tube cap) was introduced into the home cage for five minutes. We scored videos offline, blind to genotype and condition (light on or off). We measured the number of seconds the mouse spent with its nose in direct contact with the novel object or juvenile in the 180 seconds following the time the juvenile or object was introduced into the cage. In addition, we noted any aggressive-appearing behaviors toward the juvenile, freezing, and grooming behaviors. One cohort of VPA and saline mice was eliminated from analysis for aggressive behavior toward the juvenile mice. Otherwise, there were no other significant behaviors noted.

### Statistical analyses

We used the "sampsizepwr" function in MATLAB to calculate sample sizes based on preliminary data. For electrophysiology experiments, we estimated that between autism models and controls, to detect a difference in action potential firing of 25% with a standard deviation of 10 Hz, given alpha of 0.05 and power of 0.8, we required 10 cells. For photometry experiments, we estimated that between VPA mice and controls, to detect a 50% change in plateau florescence with a standard deviation of 60%, given alpha of 0.05 and power of 0.8, that we would require 12 trials in each group. For behavior / optogenetics experiments, we estimated that between light on and light off conditions, to detect a difference of 20 seconds with a standard deviation of 20 seconds, given alpha of 0.05 and power of 0.8, we required 10 animals. We therefore tested ≥10 animals in each group. Of note, our sample sizes are similar to those reported previously [16,35].

For all data analyses, we used GraphPad Prism software and custom code written in matlab. We first measured if the data were normally distributed. If they passed the D'Agostino & Pearson normality test, we used parametric statistics (Welch's t test, which does not assume equal standard deviations). If data did not pass the normality test, we used non-parametric measurements (e.g. Mann-Whitney test). All statistics were two-tailed. Using GraphPad QuickCalcs, we performed a Grubbs' test (extreme studentized deviate test) to detect if our data sets included outliers. Based on this method, none of the data sets contained significant outliers. We considered p values < 0.05 to be significant. In all figures, error bars represent ±1 standard error of the mean and * p <0.05; ** p <0.01; *** p <0.001, **** p < 0.0001. For plots of AP frequency vs. current steps, we used ANOVA to assess significance between groups. For electrophysiological recordings, data collection was not performed blind to the conditions of the experiments, but data analysis was. For behavioral and *in vivo* optogenetic experiments, animals were randomized by which experimental condition (light on vs. off) they received during the first trial, and we were blind to the experimental conditions during offline video scoring and data analysis.

## RESULTS

### In VPA mice the excitability of prefrontal L5 pyramidal neurons is abnormal

To identify possible abnormalities linked to autism in L5 of the mPFC, we first measured the intrinsic properties of mPFC L5 pyramidal neurons and fast-spiking interneurons in C57Bl/6

mice exposed to VPA or saline (SAL) *in utero*. In VPA-exposed mice, mPFC L5 pyramidal neurons tended to fire fewer action potentials in response to depolarizing current steps (Fig. S1, **top**; Table S6; SAL: n=15 cells, VPA n=19, p=0.0074, ANOVA). In contrast, the intrinsic properties of fast-spiking interneurons in L5 of mPFC were not different between VPA-exposed and control mice (Fig. S1, **bottom**; Table S6; SAL: n=19 cells, VPA n=16, p=0.51, ANOVA).

### Defects in intrinsic excitability consistently occur in subcortically-projecting (SC) but not intratelencephalic (IT) neurons

As outlined above, deep layer pyramidal neurons in the neocortex can be distinguished based on their projection targets [16–19]. In particular, L5 comprises subcortical (SC) projection neurons, which project to structures such as the MD thalamus, and intratelencephalic (IT) neurons, which project to the contralateral mPFC. These two populations can be distinguished based on their axonal targeting, intrinsic physiology, dendritic morphology, and synaptic connectivity. To determine whether the hypoexcitability we observed was generically expressed across mPFC pyramidal neurons vs. specific for a particular projection neuron subtype, we examined these non-overlapping (Fig. S2) neuronal subpopulations to evaluate their specific contributions to altered physiology in mouse models of autism.

To distinguish SC and IT cells in our recordings, prior to experiments we injected retrogradely-transported fluorescent labels into either the ipsilateral MD (to label SC cells) or contralateral mPFC (to label IT cells; Fig. 1A **and** B). In VPA-exposed mice, we found that SC cells exhibited reduced excitability while IT cells did not (Fig. 1C **and** D; Tables S1 and S2; SC – SAL: n=22, VPA n=33, p<0.0001, ANOVA; IT – SAL: n=9, VPA n=9, p=0.89, ANOVA). This indicates that the decreased excitability we initially observed in unlabeled mPFC L5 pyramidal neurons (Fig. S1) reflects specific changes in SC neurons rather than a global change throughout all L5 pyramidal projection neurons. Next, as outlined in the Introduction, to better understand the potential significance of these physiological alterations, we examined whether they might be conserved across multiple models of autism.

### Deficits in SC neuron excitability are conserved across multiple autism models

We measured the intrinsic physiology of mPFC L5 SC and IT neurons in *CNTNAP2* KO mice and *FMR1* KO mice to look for alterations like those found in VPA mice. We also studied CD1 mice exposed to VPA *in utero*, to confirm that the phenotype found in VPA C57Bl/6 mice was robust across background strains. In all four models (VPA C57Bl/6, VPA CD1, *CNTNAP2* KO, *FMR1* KO), we found that L5 SC pyramidal neurons fired significantly fewer action potentials in response to depolarizing current steps (Fig. 2A, Table S1, n=7–21 cells / group, p<0.0001–0.0057, ANOVA). In contrast, changes in the firing of intratelencephalic (IT) neurons were either not present or not consistent across these four models (Fig. 2B, Table S2, n=12–26 cells / group).

### Decreased SC neuron excitability reflects decreased input resistance

To explore possible cellular mechanisms underlying the decreased action potential firing of SC neurons, we measured passive and active membrane properties of mPFC L5 SC and IT

neurons in the autism models and control mice (Tables S1 and S2). Across all four models, we observed decreased input resistance in L5 SC cells (Fig. 2C, Table S1). Other passive membrane properties (e.g. membrane time constant, capacitance, and resting membrane potential) were not consistently altered in SC cells (Table S1). There were no consistent changes in the action potential halfwidth, spike amplitude, afterhyperpolarization, or spike-frequency adaptation in SC neurons (Fig. 2E, Tables S1 **and** S2), suggesting that changes in active conductances related to spiking do not cause the decreased firing of SC neurons we observed in autism models.

Changes in tonic inhibition or synaptic connectivity could potentially drive changes in input resistance, and altered synaptic connectivity has been reported in animal models of autism [13,28,29]. Therefore, to further explore mechanisms that could reduce the input resistance and excitability of SC neurons in VPA mice, we repeated our measures of passive and active membrane properties before and after applying blockers of excitatory and inhibitory synaptic transmission. Synaptic blockers did not change action potential firing or input resistance in SC neurons from VPA mice (Fig. S3A, n=10, p=0.66, ANOVA), suggesting that changes in synaptic input do not drive reduced SC neuron excitability, at least in VPA mice.

L5 SC neurons can be identified based on their prominent hyperpolarization-activated cation currents ($I_h$), which are mediated by hyperpolarization-activated cyclic nucleotide-gated (HCN) channels [16,18]. In SC neurons, $I_h$ gives rise to a characteristic "sag" and rebound during and following hyperpolarizing current injection. Changes in $I_h$ can alter cellular excitability [30] and have been previously described for some models of autism [14,31]. To test whether changes in $I_h$ might cause reduced SC neuron excitability, we first estimated $I_h$ by measuring the membrane potential sag and rebound elicited by a –200 pA current step (Fig. 2D). For VPA and *CNTNAP2* KO mice, there was no difference in this estimate for $I_h$ in SC neurons from autism models vs. controls. Interestingly, L5 SC neurons from *FMR1* KO mice did have significantly increased sag + rebound, relative to controls. Next, we measured the passive membrane properties and excitability of L5 SC neurons before and after applying the specific $I_h$ antagonist, ZD7288 (25 μM). Blocking $I_h$ increased input resistance but decreased action potential firing in VPA mice (Fig. S3B, n=10, p<0.0001, ANOVA). This contrasts with our observation that both input resistance and action potential firing were decreased in autism models. Finally, we estimated the resonant frequency of mPFC L5 SC pyramidal neurons, which is determined largely by $I_h$ [18] and did not observe major differences between VPA and saline control mice (Fig. S4, SAL: n=9, VPA: n=17, p=0.2463, Mann-Whitney test,). These three observations suggest that at least in VPA mice, changes in $I_h$ are not sufficient to explain altered SC neuron excitability.

In summary, our slice electrophysiology studies demonstrate a consistent cell subtype-specific reduction in the excitability and input resistance of L5 SC neurons across multiple mouse models of autism. Of course different factors may contribute to this physiological abnormality in the three autism models studied here (e.g., increased $I_h$ may be relevant in FMR1 KO mice). Nevertheless, the strikingly conserved nature of this specific physiological abnormality across diverse etiologies suggests that SC neurons may be relevant to core behavioral abnormalities in autism. This does not imply that SC neuron dysfunction is

necessarily sufficient to drive behavioral abnormalities in all cases. Furthermore, dysfunction of other cell types, e.g. IT neurons or GABAergic interneurons, may drive behavioral abnormalities in specific autism models. Nevertheless, based on our physiological findings, we decided to explore how SC neurons (or closely related subtypes of prefrontal neurons) might contribute to normal and abnormal social behavior. Specifically, we set out to measure the activity of specific prefrontal neurons during normal and abnormal social behavior using calcium imaging, and test whether optogenetic stimulation or inhibition of these neurons could elicit or ameliorate abnormal social behavior.

### Prefrontal D2Rs are expressed in L5 SC neurons but not in L5 IT or L6 CT neurons

Studying the role of SC neurons in social behavior requires the ability to preferentially express genetically encoded calcium indicators and excitatory or inhibitory opsins within SC neurons, to monitor and manipulate their activity in a cell-type specific manner. Within mPFC, neurons projecting to MD thalamus are actually more prevalent in L6 than L5; thus using a retrograde strategy (e.g., CAV2-Cre) to target SC cells rather than IT cells (as we did for our slice electrophysiology experiments), would not be adequate to differentiate thalamically-projecting SC neurons (in L5) from corticothalamic (CT) neurons in L6. Previous work from our lab suggests that L5 SC neurons should be preferentially labeled by D2-type dopamine receptors [16]. Specifically, we found that L5 SC neurons have prominent $I_h$ whereas $I_h$ is difficult to detect in L5 IT neurons [16], and L5 projection neurons with prominent $I_h$ (i.e., presumed SC cells) express D2Rs whereas L5 neurons with lower $I_h$ and L6 CT cells do not [16]. Thus, if L5 SC neurons express D2Rs, whereas L5 IT and L6 CT neurons do not, then we should be able to use D2R-Cre mice to preferentially express GCaMP or opsins in L5 SC neurons.

To validate this strategy, we injected D2R-Cre mice with adeno associated virus (AAV) encoding Cre-dependent DIO-eYFP in the right mPFC. Mice were also injected with the red fluorescent retrograde tracer CTB in either ipsilateral MD thalamus (to label L6 CT and L5 SC neurons) or contralateral mPFC (to label L5 IT neurons). We measured the percentage of L5 D2R+ cells that were also SC or IT as well as the percentage of L5 SC and IT cells that were D2R+. The majority of mPFC L5 SC neurons were also D2R+ whereas L5 IT neurons were mostly D2R negative (Fig. S5; Table S7, n=6 slices from 4 mice, p=0.0095, Mann Whitney test). Conversely, the vast majority of D2R+ neurons were located in L5 (not L6) and belonged to the SC (not IT) population (Fig. S5, Table S7). Based on these data, we concluded that it would be reasonable to use D2R-Cre mice to preferentially label L5 SC neurons (relative to L5 IT and L6 CT cells). Importantly, we also observed a smaller number of D2R+ cells in L2/3. This superficial population is smaller both in number and in soma size, suggesting it should contribute less to GCaMP signals; furthermore, for both GCaMP imaging and optogenetic experiments, we centered our viral injections and optical fibers implantations over L5 to maximize imaging / modulation of deep layer D2R+ neurons (Figs. 3B and 5B); nevertheless, throughout the following experiments, it important to remember that while highly enriched for SC neurons, the mPFC D2R+ neurons we are monitoring or manipulating do not comprise exclusively L5 SC neurons.

**Prefrontal D2R+ cells are preferentially and persistently recruited by social exploration**

To measure neuronal activity during normal social behavior, we performed bulk calcium imaging (also referred to as "fiber photometry" [32–35]) in the mPFC of wildtype mice (Fig. 3; Table S3). We stereotactically injected Cre-dependent AAV encoding the calcium indicator GCaMP6s into the mPFC of D2R-Cre mice and implanted an optical fiber above the injection site. After waiting 4–5 weeks for expression, we measured GCaMP signals from D2R+ cells using fiber photometry at baseline and during a social exploration task. In contrast to D2Rs, which are preferentially expressed on L5 SC neurons, D1Rs are more broadly expressed throughout the mPFC, including both SC and IT cells [16,19]. Therefore, as a comparison, we also measured GCaMP signals from D1R+ mPFC neurons using a separate cohort of D1R-Cre mice.

To assay social behavior, we measured the time a subject mouse spent exploring a novel juvenile mouse of the same sex introduced to its home cage. Separately, we measured the amount of time the subject mouse spent exploring a novel object introduced to its home cage [6,35]. We measured the average baseline fluorescence, then quantified the change in fluorescence following the introduction of the juvenile mouse or novel object. For both D2R + (primarily SC) and D1R+ (mixed SC and IT) mPFC neurons, we observed pronounced increases in fluorescence during the first interaction between the adult and juvenile or the novel object (Fig. 3). The increase in ΔF/F was significantly larger in the D2R population than the D1R population over the first 10 seconds of social interaction (n = 12/20 D1R/D2R recordings, p = 0.004, Mann-Whitney test). By contrast, during novel object exploration signals in these two populations were not significantly different (n = 12/18 D1R/D2R recordings, p = 0.69, Mann-Whitney test). For D2R+ neurons, the increase in fluorescence was greater during social exploration than novel object exploration (10.7 ± 1.5% for social vs. 4.7 ± 1.5% for novel object, comparing the 10 sec following the interaction to the period −15 to −5 sec before the interaction, n = 20/18 for social/novel; p = 0.003, Mann-Whitney test). In contrast, for D1R-expressing neurons, the increase in fluorescence was not significantly different during social and novel object exploration.

Interestingly, following the adult's first interaction with the juvenile, there was an extended period (~100 seconds) during which ΔF/F in D2R-expressing neurons remained significantly higher than in D1R–expressing neurons (n = 12/20 D1R/D2R recordings, p = 0.012, Mann-Whitney test). This difference did not appear during novel object exploration (n = 12/18 D1R/D2R recordings, p = 0.85, Mann-Whitney test). To determine whether this prolonged "plateau" of activity was driven by (or independent of) subsequent interactions, we compared ΔF/F during epochs in which the adult is engaging in social or novel-object exploration with epochs in which the mouse is not interacting. Looking at epochs >30 seconds after the first interaction, during the social task, ΔF/F in D2R+ neurons was not significantly different depending on whether the mouse was exploring or not (p = 0.77, W = 113, Wilcoxon sign-rank test). By contrast, during the novel-object task, D2R+ neuron ΔF/F was significantly higher during periods of active exploration (p = 0.003, W = 11, Wilcoxon sign-rank text). These results show that D2R+ neurons maintain activity when the juvenile is present, even when the animals are not actively interacting.

Thus, D2R+ neuron responses are greater in magnitude and duration for social exploration than novel object objection, and during social exploration, responses of D2R+ neurons are greater in magnitude and duration than those of D1R+ neurons. In other words, D2R+ neurons (which are highly overlapping with the SC population) are preferentially and persistently recruited by social exploration, whereas other populations of mPFC neurons (D1R+ neurons) are not.

### The recruitment of mPFC D2R+ neurons by social exploration is abnormal in VPA mice

To confirm that the prolonged GCaMP signal observed in D2R+ neurons following an initial social interaction reflects neuronal activity, not just GCaMP kinetics, we repeated the experiment in saline-exposed (control) mice using the genetically encoded calcium indicator GCaMP6f, which has faster kinetics than GCaMP6s [36]. Once again, in control mice, GCaMP signals from mPFC D2R+ cells exhibited a prolonged elevation that lasted ~100 seconds after an initial social interaction (Fig. 4) and did not occur following novel object exploration.

Given that SC cells, which comprise the bulk of mPFC D2R+ neurons, have abnormal excitability in multiple autism models (Fig. 2), we wondered whether social exploration-driven signals from D2R+ neurons would be altered in an autism model. We specifically decided to explore this question using VPA mice, simply because in the assay described above, we observed decreased social exploration for VPA mice, but not CNTNAP2 or FMR1 KO mice (Fig. S6). We exposed D2R-Cre mice to VPA or saline *in utero*, then performed fiber photometry to measure GCaMP6f signals from mPFC D2R+ neurons. VPA mice did exhibit a transient increase in GCaMP signal when they first sniffed the novel juvenile, but instead of a persistent elevation, this signal rapidly decayed back to baseline (Fig. 4; Table S4, n=28/18 VPA/SAL recordings, p=0.0001, Mann-Whitney test). Thus, prefrontal D2R+ neurons, which are preferentially recruited by social exploration, exhibit abnormal recruitment during social exploration in VPA mice.

### Optogenetic manipulations of D2R+ neurons bidirectionally modulate social behavior

To test whether D2R+ neurons play a causal role in normal or abnormal social behavior, we stereotactically injected AAV into mPFC to drive Cre-dependent expression of the inhibitory opsin halorhodopsin (eNpHR) or the excitatory opsin channelrhodopsin (ChR2) in D2R-Cre mice exposed to VPA *in utero* or control (not VPA-exposed) mice, and implanted fiber optic cannulas. We then selectively inhibited or excited D2R+ prefrontal neurons during social exploration and novel object exploration. For each mouse, we performed the assay two times (separated by at least 6 days), once in the presence and once in the absence of light stimulation; the order of experiments (light on or off) was randomized and counterbalanced across mice, and we performed within mouse comparisons. Importantly, the amount of time an individual mouse engages in social exploration is highly variable[35] and depends on many aspects of the housing and testing conditions. Therefore, comparisons between different groups of mice should only be made when those two groups were adequately powered and closely matched, i.e., bred, housed, and tested at the same time under identical conditions. This was the case, for example, when we compared social exploration in VPA and saline mice (Fig. S6), but was not the case for the different groups shown in Fig. 5, which were

often tested several months apart. Photometry experiments in VPA and saline mice (Fig. 4) also used mice that were bred, housed, and tested concurrently.

In VPA mice, optogenetic inhibition of mPFC SC neurons *increased* social interaction (the amount of time VPA mice spend exploring novel juvenile mice) by >20%, but had no significant effect on novel object exploration (Fig. 5, Table S5, n=10, p=0.03, Welch's two-tailed t test). In control mice, we observed no increase in social behavior following optogenetic inhibition of mPFC D2R+ cells (n=11, p=0.30, Welch's two-tailed t test). This suggests that the pro-social effects of inhibiting D2R-expressing mPFC neurons reflect the suppression of abnormal activity that is present in VPA-exposed mice but not in controls. Furthermore, VPA mice in which halorhodopsin was broadly expressed in the mPFC using the pan-neuronal promoter synapsin exhibited no enhancement of social or novel object exploration between light on and off conditions; in fact, social exploration was decreased in these animals (Fig. 5, Table S5, n=11, p=0.03, Welch's two tailed t test). This shows that in VPA mice, the pro-social effects of optogenetic inhibition in the mPFC are cell-subtype specific and do not generalize to nonspecific inhibition. Conversely, in both control and VPA mice, acute optogenetic stimulation at 10 Hz using ChR2 in D2R-Cre mice decreased social exploration and tended to increase novel object exploration (though changes in novel object exploration did not reach statistical significance). Thus, consistent with our hypothesis, optogenetic manipulations that target a specific population of D2R+ neurons can elicit social deficits in control mice, and exacerbate (stimulation) or ameliorate (inhibition) social deficits in a mouse model of autism.

## DISCUSSION

Deep layer (L5/6) projection neurons within PFC represent the strongest locus for genetic convergence in autism [7], but specific abnormalities within these neurons that contribute to abnormal behavior in autism have been elusive. Here we identified a specific subtype of deep layer prefrontal projection neurons – SC neurons – that exhibit conserved abnormalities (reduced input resistance and excitability) across multiple models of autism. Then we showed that prefrontal D2R+ neurons are preferentially recruited during normal social behavior, abnormally recruited by social behavior in a mouse model of autism, and can be targeted to either reproduce, exacerbate, or ameliorate autism-associated social deficits. As noted above, in the mPFC, the D2R+ and SC neuron populations are largely overlapping; our optical fibers targeted the deep prefrontal layers, where D2R expression is largely confined to SC neurons, and most SC neurons are D2R+.

Three aspects of these results are particularly noteworthy. First, they suggest that abnormalities in prefrontal SC neurons are likely present in many forms of autism. Second, prefrontal D2R+ neurons are more strongly recruited by social than novel object exploration, and stimulating these neurons elicits distinct effects on social vs. novel object exploration, suggesting that D2R+ neurons play some kind of specific role in social interaction as opposed to a generic role in all exploratory behaviors. Third, inhibiting prefrontal D2R+ neurons improved social behavior in VPA mice, whereas nonspecific inhibition of prefrontal neurons did not. Taken together, these results suggest that abnormalities in SC / D2R+

neurons in mPFC may contribute to social deficits in autism, and conversely that targeting these cells may be a particularly effective way to ameliorate those deficits.

## Caveats and future directions

Even though SC neuron hypoexcitability occurs in VPA mice, *FMR1* KO mice, and *CNTNAP2* KO mice, we did not observe deficits in our social exploration assay for *FMR1* or *CNTNAP2* KO mice (Fig. S6). This suggests that SC neuron abnormalities do not invariably drive social deficits under all conditions. Additional abnormalities present in VPA mice may contribute to social deficits. Alternatively, compensations present in *FMR1* or *CNTNAP2* KO mice may prevent the emergence of SC neuron-induced social deficits in this particular assay. In other words, while abnormalities in prefrontal SC / D2R+ neurons may be one mechanism contributing to social deficits in autism, other factors must also play key roles.

Although prefrontal SC / D2R+ neurons seem to be abnormal in autism models and involved in social behavior, we have not identified a simple monotonic relationship between activity in SC / D2R+ neurons and behavior. That is, in autism models, SC neurons are hypoexcitable and D2R+ neurons are less active during social behavior in VPA mice. However, inhibiting D2R+ neurons in VPA mice increases social exploration. This argues against a simple model in which higher or lower SC neuron activity drives increased or decreased social interaction. This is not surprising given that neurons in the mPFC typically exhibit complex firing patterns that reflect the conjunction of multiple task-relevant stimuli and parameters [37–39]. Thus a more conservative interpretation that is consistent with our observations and the complexity of prefrontal circuits is as follows: in VPA mice, the encoding of social interactions is altered in mPFC D2R+ neurons, and suppressing the abnormal activity of this neuronal population enhances social behavior; the hypoexcitability of SC neurons is likely related to this abnormal *in vivo* activity, though the exact nature of this relationship (contributory vs. compensatory vs. other) remains unknown.

We have not determined the precise cellular mechanisms which drive reduced SC neuron excitability and input resistance. At least in VPA mice, these do not appear to involve HCN channels or synaptic transmission. Rather than drilling further into these mechanisms, we chose to investigate how a closely related population of prefrontal neurons (D2R+ neurons) contribute to social behavior *in vivo*. Future work, beyond the scope of the current study, will pinpoint the ionic or structural basis for altered SC neuron physiology.

In behavioral studies we used D2R-Cre mice and the placement of our optical fibers to preferentially target L5 SC neurons. However, D2Rs are expressed not only by L5 SC neurons but also by L2/3 neurons (Fig. S5) and some interneurons [40]. As such, our experiments surely included other populations of D2R+ neurons. Thus, our results – that prefrontal D2R+ neurons are preferentially recruited by social exploration (unlike D1R+ neurons), and can be targeted to improve social exploration in VPA mice (whereas nonspecific targeting of mPFC neurons is ineffective) – represent valuable starting points for the field. But it will be important for future studies, using improved methods for labeling specific neuronal populations, to clarify exactly how SC neurons vs. other D2R+ populations

contribute to the GCaMP signals and behavioral effects of optogenetic manipulations observed here.

Our behavioral measures do not capture all of the nuances of what is already a highly simplified social assay. Nevertheless, this experimental paradigm does highlight deficits in social interest, a core challenge for many people with autism. Finally, our optogenetic and calcium imaging studies targeted both prelimbic (PL) and infralimbic (IL) cortices. As differences have been observed between PL and IL in terms of connectivity and roles in behavior [41], future studies which selectively target PL or IL may refine our results.

### The mPFC and MD thalamus in autism

The mPFC shares rich reciprocal connections with the MD thalamus [42–47], a region implicated in learning and memory, cognitive flexibility, and corollary discharge [48–54]. Several pieces of evidence suggest that changes in thalamic volume [55,56] as well as changes in the structural [10,11,57] and functional [11] connectivity between PFC and MD occur in human autism. Thus, the electrophysiological changes we observed in mPFC SC neurons represent a potential mechanism for decreases in PFC-MD functional connectivity associated with human autism.

### Relationship to the excitatory/inhibitory imbalance hypothesis of autism

A prominent hypothesis is that an excess of excitatory neuronal activity relative to neuronal inhibition ("E/I imbalance") leads to the core clinical features of autism along with associated findings such as hyperactivity, epileptiform activity, and epilepsy [58,59]. One straightforward prediction based on this hypothesis is that pyramidal neurons should be hyperexcitable in mouse models of autism compared to controls [14,60]. In contrast, the electrophysiology data presented here suggest that in the autism models we studied, mPFC L5 SC neurons are intrinsically hypoexcitable due to a reduction in their input resistance. A key caveat is that the intrinsic hypoexcitability we found should not be interpreted in isolation. Specifically, we do not know, for example, whether L5 SC neurons receive excessive excitatory synaptic input, which outweighs their intrinsic hypoexcitability; indeed, intrinsic hypoexcitability may represent a compensation for synaptic or circuit-level abnormalities.

### Relationship to previous physiological studies

Changes in the electrophysiological properties and synaptic connectivity of L5 neocortical pyramidal neurons have been demonstrated in individual rodent models of autism [13–15,28,61], with diverse results. For example, in *FMR1* KO mice, somatosensory cortex L5 pyramidal neurons had deficits in dendritic but not somatic excitability; this was related to changes in dendritic $I_h$ [61]. In this same model, prefrontal L5 PT neurons had normal somatic input resistance, but displayed decreased $I_h$ at the soma and dendrites [14]. In juvenile VPA mice, L5 neurons did not have altered intrinsic membrane properties, but had higher probability of local synaptic connections; these connections were weaker than in control mice [13]. Of note, these changes were observed in L5 neurons which, like SC neurons, had thick apical tufts. This implies that electrophysiological defects start early in development and persist into adulthood. In a conditional *MET* knockout model, frontal L5 corticostriatal (but not

corticopontine) neurons received increased local inputs but did not differ in their intrinsic electrophysiological properties [15]. In *MECP2* knockout mice, primary somatosensory cortex L5 pyramidal neurons had decreased spontaneous firing rates, but did not differ in their intrinsic properties compared to wildtype controls [62]. In addition to this literature examining cortical changes in individual autism models, extensive work has been done examining the changes in the electrophysiological properties of hippocampal neurons and other subcortical structures in individual autism models [63]. Our study also builds upon others that have examined electrophysiological abnormalities associated with autism in more than one animal model [64,65].

Importantly, a previous study used optogenetic stimulation in the mPFC to disrupt social behavior in wild-type mice and showed that this effect was ameliorated by the concomitant stimulation of interneurons [6]. Whereas that study mitigated social deficits that were induced by optogenetic excitation in wild-type mice, here we use a cell-type specific optogenetic manipulation to rescue social deficits in an established mouse model of autism.

## Conclusion

Despite limitations, we have demonstrated that a specific population of mPFC neurons exhibits a consistent physiological defect across multiple models of autism, and linked a highly overlapping population to both normal social behavior and social deficits in an animal of autism. These findings identify specific circuits within the mPFC as potential therapeutic target for social deficits, a core symptom of autism for which there are no current medical treatments. Elucidating pathways that are either upstream of autism-associated abnormalities in subcortically projecting mPFC neurons or downstream of their synaptic targets, and/or devising additional ways (besides D2R-expression) to preferentially target these neurons may lead to novel circuit-based approaches for understanding and treating the social deficits at the heart of this disorder.

## Supplementary Material

Refer to Web version on PubMed Central for supplementary material.

## Acknowledgments

## REFERENCES

1. Centers for Disease Control and Prevention. Prevalence of autism spectrum disorders - Autism and Developmental Disabilities Monitoring Network, 14 sites, United States, 2008. Morb Mortal Wkly Rep 2012; 61: 1–19.

2. Baron-Cohen S, Ring H, Moriarty J, Schmitz B, Costa D, Ell P. Recognition of mental state terms. Clinical findings in children with autism and a functional neuroimaging study of normal adults. Br J Psychiatry 1994; 165: 640–649. [PubMed: 7866679]

3. Castelli F, Frith C, Happé F, Frith U. Autism, Asperger syndrome and brain mechanisms for the attribution of mental states to animated shapes. Brain 2002; 125: 1839–1849. [PubMed: 12135974]

4. Bachevalier J, Mishkin M. Visual recognition impairment follows ventromedial but not dorsolateral prefrontal lesions in monkeys. Behav Brain Res 1986; 20: 249–61. [PubMed: 3741586]

5. Morgan MA, Romanski LM, LeDoux JE. Extinction of emotional learning: contribution of medial prefrontal cortex. Neurosci Lett 1993; 163: 109–13. [PubMed: 8295722]

6. Yizhar O, Fenno LE, Prigge M, Schneider F, Davidson TJ, O'Shea DJ et al. Neocortical excitation/inhibition balance in information processing and social dysfunction. Nature 2011; 477: 1–8.

7. Willsey AJ, Sanders SJ, Li M, Dong S, Tebbenkamp AT, Muhle RA et al. Coexpression networks implicate human midfetal deep cortical projection neurons in the pathogenesis of autism. Cell 2013; 155: 997–1007. [PubMed: 24267886]

8. Happé F, Ehlers S, Fletcher P, Frith U, Johansson M, Gillberg C et al. 'Theory of mind' in the brain. Evidence from a PET scan study of Asperger syndrome. Neuroreport 1996; 8: 197–201. [PubMed: 9051780]

9. Pierce K, Haist F, Sedaghat F, Courchesne E. The brain response to personally familiar faces in autism: findings of fusiform activity and beyond. Brain 2004; 127: 2703–16. [PubMed: 15319275]

10. Cheon KA, Kim YS, Oh SH, Park SY, Yoon HW, Herrington J et al. Involvement of the anterior thalamic radiation in boys with high functioning autism spectrum disorders: A Diffusion Tensor Imaging study. Brain Res 2011; 1417: 77–86. [PubMed: 21890117]

11. Nair A, Treiber JM, Shukla DK, Shih P, Müller R-A. Impaired thalamocortical connectivity in autism spectrum disorder: a study of functional and anatomical connectivity. Brain 2013; 136: 1942–55. [PubMed: 23739917]

12. Testa-Silva G, Loebel A, Giugliano M, de Kock CPJ, Mansvelder HD, Meredith RM. Hyperconnectivity and slow synapses during early development of medial prefrontal cortex in a mouse model for mental retardation and autism. Cereb Cortex 2012; 22: 1333–42. [PubMed: 21856714]

13. Rinaldi T, Perrodin C, Markram H, Cauli B, Pierre U. Hyper-connectivity and hyper-plasticity in the medial prefrontal cortex in the valproic Acid animal model of autism. Front Neural Circuits 2008; 2: 4. [PubMed: 18989389]

14. Kalmbach BE, Johnston D, Brager DH. Cell-Type Specific Channelopathies in the Prefrontal Cortex of the fmr1-/y Mouse Model of Fragile X Syndrome. eNeuro 2015; 2: ENEURO.0114–15.2015.

15. Qiu S, Anderson CT, Levitt P, Shepherd GMG. Circuit-specific intracortical hyperconnectivity in mice with deletion of the autism-associated Met receptor tyrosine kinase. J Neurosci 2011; 31: 5855–64. [PubMed: 21490227]

16. Gee S, Ellwood I, Patel T, Luongo F, Deisseroth K, Sohal VS. Synaptic activity unmasks dopamine D2 receptor modulation of a specific class of layer V pyramidal neurons in prefrontal cortex. J Neurosci 2012; 32: 4959–71. [PubMed: 22492051]

17. Lee AT, Gee SM, Vogt D, Patel T, Rubenstein JL, Sohal VS. Pyramidal neurons in prefrontal cortex receive subtype-specific forms of excitation and inhibition. Neuron 2014; 81: 61–8. [PubMed: 24361076]

18. Dembrow NC, Chitwood RA, Johnston D. Projection-specific neuromodulation of medial prefrontal cortex neurons. J Neurosci 2010; 30: 16922–37. [PubMed: 21159963]

19. Seong HJ, Carter AG. D1 Receptor Modulation of Action Potential Firing in a Subpopulation of Layer 5 Pyramidal Neurons in the Prefrontal Cortex. J. Neurosci 2012; 32: 10516–10521. [PubMed: 22855801]

20. Moore SJ, Turnpenny P, Quinn A, Glover S, Lloyd DJ, Montgomery T et al. A clinical study of 57 children with fetal anticonvulsant syndromes. J Med Genet 2000; 37: 489–97. [PubMed: 10882750]

21. Christensen J, Grønborg TK, Sørensen MJ, Schendel D, Parner ET, Pedersen LH et al. Prenatal valproate exposure and risk of autism spectrum disorders and childhood autism. JAMA 2013; 309: 1696–703. [PubMed: 23613074]

22. Schneider T, Przewłocki R. Behavioral alterations in rats prenatally exposed to valproic acid: animal model of autism. Neuropsychopharmacology 2005; 30: 80–9. [PubMed: 15238991]

23. Strauss KA, Puffenberger EG, Huentelman MJ, Gottlieb S, Dobrin SE, Parod JM et al. Recessive symptomatic focal epilepsy and mutant contactin-associated protein-like 2. N Engl J Med 2006; 354: 1370–1377. [PubMed: 16571880]

24. Verkerk A, Pieretti M, Sutcliffe J, Fu Y. Identification of a gene (FMR-1) containing a CGG repeat coincident with a breakpoint cluster region exhibiting length variation in fragile X syndrome. Cell 1991; 65: 905–914. [PubMed: 1710175]

25. Peñagarikano O, Abrahams BSS, Herman EII, Winden KDD, Gdalyahu A, Dong H et al. Absence of CNTNAP2 leads to epilepsy, neuronal migration abnormalities, and core autism-related deficits. Cell 2011; 147: 235–46. [PubMed: 21962519]

26. The Dutch-Belgian Fragile X Consortium. Fmr1 knockout mice: a model to study fragile X mental retardation. Cell 1994; 78: 23–33. [PubMed: 8033209]

27. Spencer CM, Alekseyenko O, Serysheva E, Yuva-Paylor LA, Paylor R. Altered anxiety-related and social behaviors in the Fmr1 knockout mouse model of fragile X syndrome. Genes Brain Behav 2005; 4: 420–30. [PubMed: 16176388]

28. Rinaldi T, Silberberg G, Markram H. Hyperconnectivity of local neocortical microcircuitry induced by prenatal exposure to valproic acid. Cereb Cortex 2008; 18: 763–70. [PubMed: 17638926]

29. Zhang S, Xu M, Kamigaki T, Hoang Do JP, Chang W-C, Jenvay S et al. Long-range and local circuits for top-down modulation of visual cortex processing. Science (80- ) 2014; 345: 660–665.

30. Shah MM. Hyperpolarization-Activated Cyclic Nucleotide-Gated Channel Currents in Neurons. Cold Spring Harb Protoc 2016; 2016: pdb.top087346.

31. Yi F, Yi F, Danko T, Botelho SC, Patzke C, Pak C et al. Autism-associated SHANK3 haploinsufficiency causes I h channelopathy in human neurons. 2016; 2669. doi:10.1126/science.aaf2669.

32. Adelsberger H, Garaschuk O, Konnerth A. Cortical calcium waves in resting newborn mice. Nat Neurosci 2005; 8: 988–90. [PubMed: 16007081]

33. Cui G, Jun SB, Jin X, Pham MD, Vogel SS, Lovinger DM et al. Concurrent activation of striatal direct and indirect pathways during action initiation. Nature 2013; 494: 238–42. [PubMed: 23354054]

34. Cui G, Jun SB, Jin X, Luo G, Pham MD, Lovinger DM et al. Deep brain optical measurements of cell type-specific neural activity in behaving mice. Nat Protoc 2014; 9: 1213–28. [PubMed: 24784819]

35. Gunaydin LA, Grosenick L, Finkelstein JC, Kauvar IV, Fenno LE, Adhikari A et al. Natural neural projection dynamics underlying social behavior. Cell 2014; 157: 1535–51. [PubMed: 24949967]

36. Chen T-W, Wardill TJ, Sun Y, Pulver SR, Renninger SL, Baohan A et al. Ultrasensitive fluorescent proteins for imaging neuronal activity. Nature 2013; 499: 295–300. [PubMed: 23868258]

37. Karlsson MP, Tervo DGR, Karpova AY. Network resets in medial prefrontal cortex mark the onset of behavioral uncertainty. Science 2012; 338: 135–9. [PubMed: 23042898]

38. Hyman JM, Ma L, Balaguer-Ballester E, Durstewitz D, Seamans JK. Contextual encoding by ensembles of medial prefrontal cortex neurons. Proc Natl Acad Sci 2012; 109: 5086–5091. [PubMed: 22421138]

39. Ma L, Hyman JM, Durstewitz D, Phillips AG, Seamans JK. A Quantitative Analysis of Context-Dependent Remapping of Medial Frontal Cortex Neurons and Ensembles. J Neurosci 2016; 36: 8258–8272. [PubMed: 27488644]

40. Tritsch NX, Sabatini BL. Dopaminergic Modulation of Synaptic Transmission in Cortex and Striatum. Neuron 2012; 76: 33–50. [PubMed: 23040805]

41. Adhikari A, Lerner TN, Finkelstein J, Pak S, Jennings JH, Davidson TJ et al. Basomedial amygdala mediates top-down control of anxiety and fear. Nature 2015; 527: 179–185. [PubMed: 26536109]

42. Krettek JE, Price JL. The cortical projections of the mediodorsal nucleus and adjacent thalamic nuclei in the rat. J Comp Neurol 1977; 171: 157–191. [PubMed: 64477]

43. Groenewegen HJ. Organization of the afferent connections of the mediodorsal thalamic nucleus in the rat, related to the mediodorsal-prefrontal topography. Neuroscience 1988; 24: 379–431. [PubMed: 2452377]

44. Ray JP, Price JL. The organization of the thalamocortical connections of the mediodorsal thalamic nucleus in the rat, related to the ventral forebrain-prefrontal cortex topography. J Comp Neurol 1992; 323: 167–197. [PubMed: 1401255]

45. Ray JP, Price JL. The organization of projections from the mediodorsal nucleus of the thalamus to orbital and medial prefrontal cortex in macaque monkeys. J Comp Neurol 1993; 31: 1–31.

46. Goldman-Rakic PS, Porrino LJ. The primate mediodorsal (MD) nucleus and its projection to the frontal lobe. J Comp Neurol 1985; 242: 535–560. [PubMed: 2418080]

47. Conde F, Audinat E, Maire-Lepoivre E, Crepel F. Afferent connections of the medial frontal cortex of the rat. A study using retrograde transport of fluorescent dyes. I. Thalamic afferents. Brain Res Bull 1990; 24: 341–354. [PubMed: 2337814]

48. Parnaudeau S, Taylor K, Bolkan SS, Ward RD, Balsam PD, Kellendonk C. Mediodorsal Thalamus Hypofunction Impairs Flexible Goal-Directed Behavior. Biol Psychiatry 2014; : 1–9.

49. Parnaudeau S, O'Neill P-K, Bolkan SS, Ward RD, Abbas AI, Roth BL et al. Inhibition of mediodorsal thalamus disrupts thalamofrontal connectivity and cognition. Neuron 2013; 77: 1151–62. [PubMed: 23522049]

50. Bellebaum C, Daum I, Koch B, Schwarz M, Hoffmann KP. The role of the human thalamus in processing corollary discharge. Brain 2005; 128: 1139–1154. [PubMed: 15758033]

51. Crapse TB, Sommer MA. Corollary discharge across the animal kingdom. Nat Rev Neurosci 2008; 9: 587–600. [PubMed: 18641666]

52. Baxter MG. Mediodorsal thalamus and cognition in non-human primates. Front Syst Neurosci 2013; 7: 38. [PubMed: 23964206]

53. Browning PGF, Chakraborty S, Mitchell AS. Evidence for Mediodorsal Thalamus and Prefrontal Cortex Interactions during Cognition in Macaques. Cereb Cortex 2015; : 1–16. [PubMed: 23926113]

54. Golden EC, Graff-Radford J, Jones DT, Benarroch EE. Mediodorsal nucleus and its multiple cognitive functions. Neurology 2016; 87: 2161–2168. [PubMed: 27770073]

55. Tsatsanis KD, Rourke BP, Klin A, Volkmar FR, Cicchetti D, Schultz RT. Reduced thalamic volume in high-functioning individuals with autism. Biol Psychiatry 2003; 53: 121–129. [PubMed: 12547467]

56. Tamura R, Kitamura H, Endo T, Hasegawa N, Someya T. Reduced thalamic volume observed across different subgroups of autism spectrum disorders. Psychiatry Res 2010; 184: 186–8. [PubMed: 20850279]

57. Tan GCY, Doke TF, Ashburner J, Wood NW, Frackowiak RSJ. Normal variation in fronto-occipital circuitry and cerebellar structure with an autism-associated polymorphism of CNTNAP2. Neuroimage 2010; 53: 1030–1042. [PubMed: 20176116]

58. Rubenstein JLR, Merzenich MM. Model of autism: increased ratio of excitation/inhibition in key neural systems. Genes Brain Behav 2003; 2: 255–67. [PubMed: 14606691]

59. Nelson SB, Valakh V. Excitatory/Inhibitory Balance and Circuit Homeostasis in Autism Spectrum Disorders. Neuron 2015; 87: 684–98. [PubMed: 26291155]

60. Gibson JR, Bartley AF, Hays S a, Huber KM. Imbalance of neocortical excitation and inhibition and altered UP states reflect network hyperexcitability in the mouse model of fragile X syndrome. J Neurophysiol 2008; 100: 2615–26. [PubMed: 18784272]

61. Zhang Y, Bonnan A, Bony G, Ferezou I, Pietropaolo S, Ginger M et al. Dendritic channelopathies contribute to neocortical and sensory hyperexcitability in Fmr1-/y mice. Nat Neurosci 2014; 17: 1701–1709. [PubMed: 25383903]

62. Dani VS, Chang Q, Maffei A, Turrigiano GG, Jaenisch R, Nelson SB. Reduced cortical activity due to a shift in the balance between excitation and inhibition in a mouse model of Rett syndrome. Proc Natl Acad Sci U S A 2005; 102: 12560–5. [PubMed: 16116096]

63. Brager DH, Akhavan AR, Johnston D. Impaired Dendritic Expression and Plasticity of h-Channels in the fmr1-/y Mouse Model of Fragile X Syndrome. Cell Rep 2012; 1: 225–233. [PubMed: 22662315]

64. Tyzio R, Nardou R, Ferrari DC, Tsintsadze T, Shahrokhi A, Eftekhari S et al. Oxytocin-mediated GABA inhibition during delivery attenuates autism pathogenesis in rodent offspring. Science 2014; 343: 675–9. [PubMed: 24503856]

65. Luongo FJ, Horn ME, Sohal VS. Putative microcircuit-level substrates for attention are disrupted in mouse models of autism. Biol Psychiatry 2016; 79: 667–675. [PubMed: 26022075]

66. Murdoch JD, Gupta AR, Sanders SJ, Walker MF, Keaney J, Fernandez TV. et al. No evidence for association of autism with rare heterozygous point mutations in Contactin-Associated Protein-Like 2 (CNTNAP2), or in Other Contactin-Associated Proteins or Contactins. PLoS Genet 2015; 11: e1004852. [PubMed: 25621974]

67. Gogolla N, Leblanc JJ, Quast KB, Südhof T, Fagiolini M, Hensch TK. Common circuit defect of excitatory-inhibitory balance in mouse models of autism. J Neurodev Disord 2009; 1: 172–181. [PubMed: 20664807]

68. Yona G, Meitav N, Kahn I, Shoham S. Realistic Numerical and Analytical Modeling of Light Scattering in Brain Tissue for Optogenetic Applications. eNeuro 2016; 3: ENEURO.0059–15.2015.
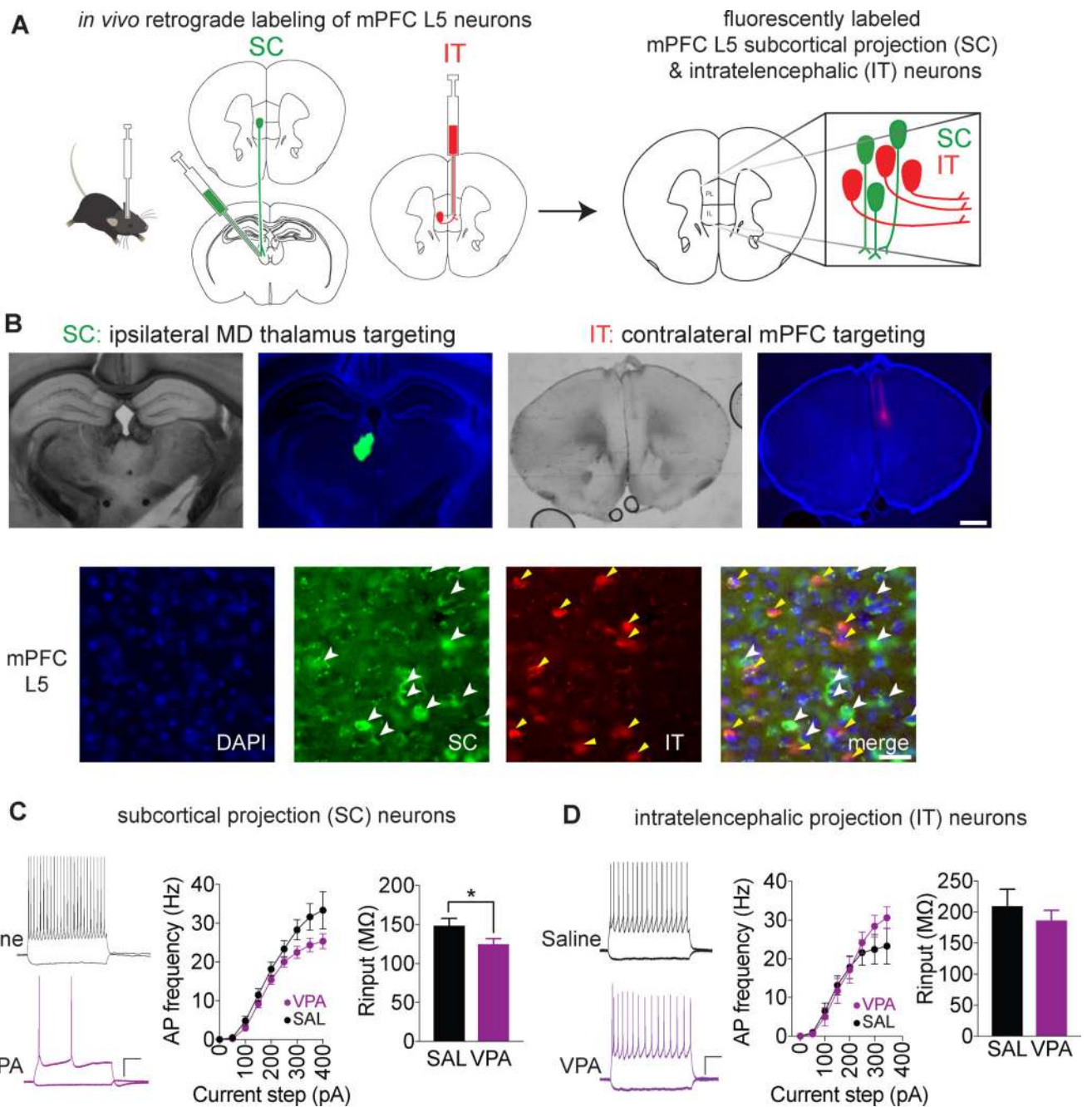
**Figure 1. Prenatal VPA exposure causes deficits in the excitability of mPFC L5 subcortical projection (SC) pyramidal neurons.**
**A.** Retrograde labeling of mPFC L5 SC cells by injection of CTB in ipsilateral mediodorsal (MD) thalamus and labeling of mPFC L5 intratelencephalic projection (IT) neurons by injection of CTB in contralateral mPFC. **B.** Photomicrographs of injection sites (**top**, 2x magnification) and labeled cells (**bottom**, arrowheads). Scale bars = 1 mm and 100 μm. **C** and **D.** Current clamp recordings from VPA exposed (purple) and saline control mice (black) in response to current steps in mPFC L5 SC (**C**) and IT (**D**) neurons. Examples show

responses to −50 and +200 pA steps. Scale bars = 200 ms, 20 mV. VPA = Valproic Acid, SAL = saline control. PL, Prelimbic cortex. IL, Infralimbic cortex.
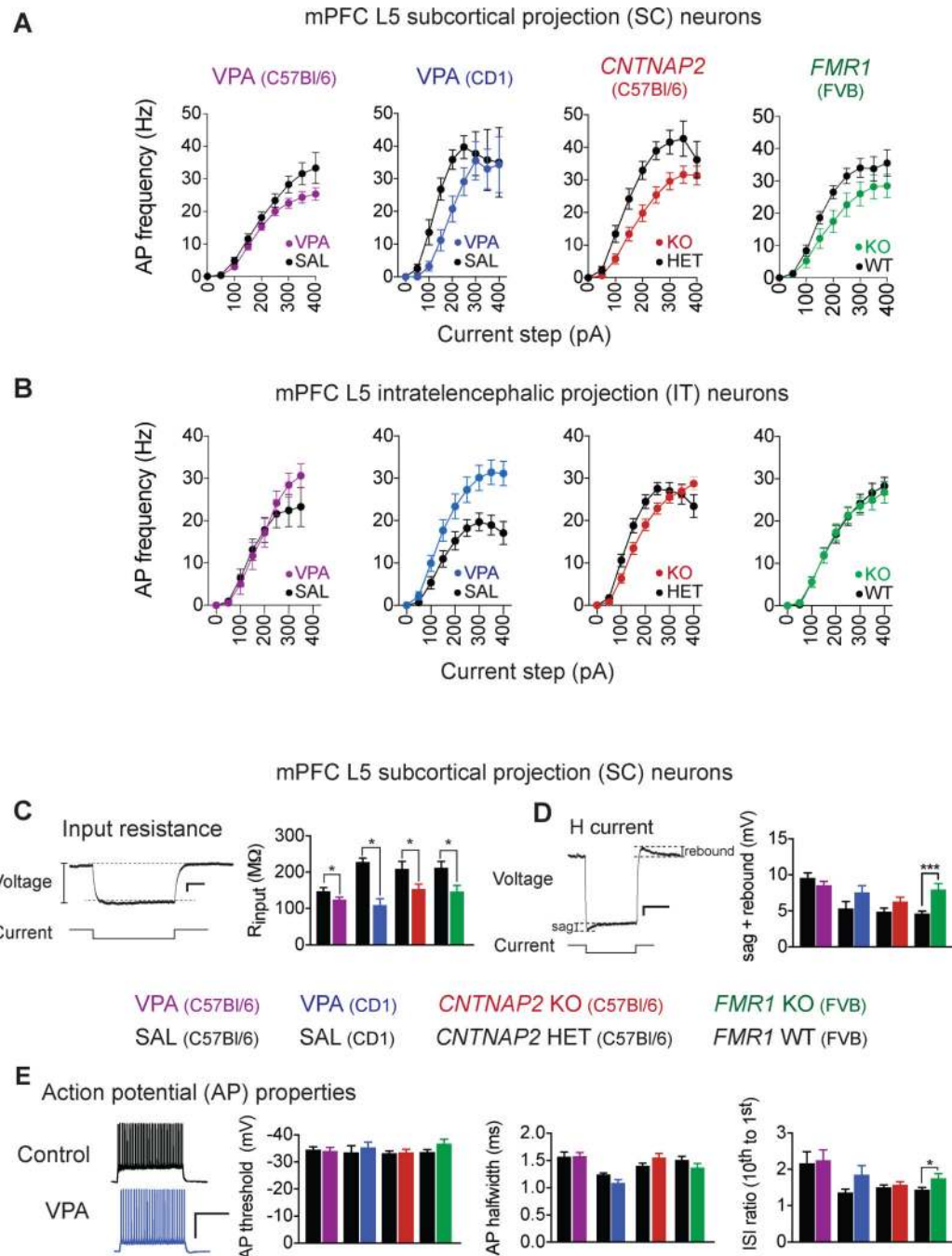
**Figure 2. Prenatal VPA exposure, *FMR1* KO, and *CNTNAP2* KO all cause a deficit in the excitability of mPFC L5 subcortical projection (SC) pyramidal neurons, which is associated with decreased input resistance.**
**A.** In mPFC L5 SC neurons, action potential (AP) frequency in response to current injection in autism models (colored circles) compared to controls (black). Background strains are shown in parentheses. **B.** Same as A, but in IT neurons. **C**, Input resistance in autism models and controls calculated based on the voltage deflection to a −50 pA current step. Scale bar: 2 mV, 50 pA, 200 ms. **D**, H current in autism models and controls estimated by the sum of the sag and rebound voltage deflections in response to a −200 pA current step. Scale bar: 2 mV,

250 pA, 500 ms. **E**, Action potential threshold, halfwidth, and spike frequency adaptation in autism models and controls. ISI: interspike interval. Scale bar: = 500 ms, 50 mV.VPA = Valproic Acid, SAL = saline control, KO = knockout, HET = heterozygote, WT = wild type. PL, Prelimbic cortex. IL, Infralimbic cortex. For C57Bl/6 VPA & SAL, f/i curves (A, B) and input resistance bar graph (C) are re-presented from Fig. 1.
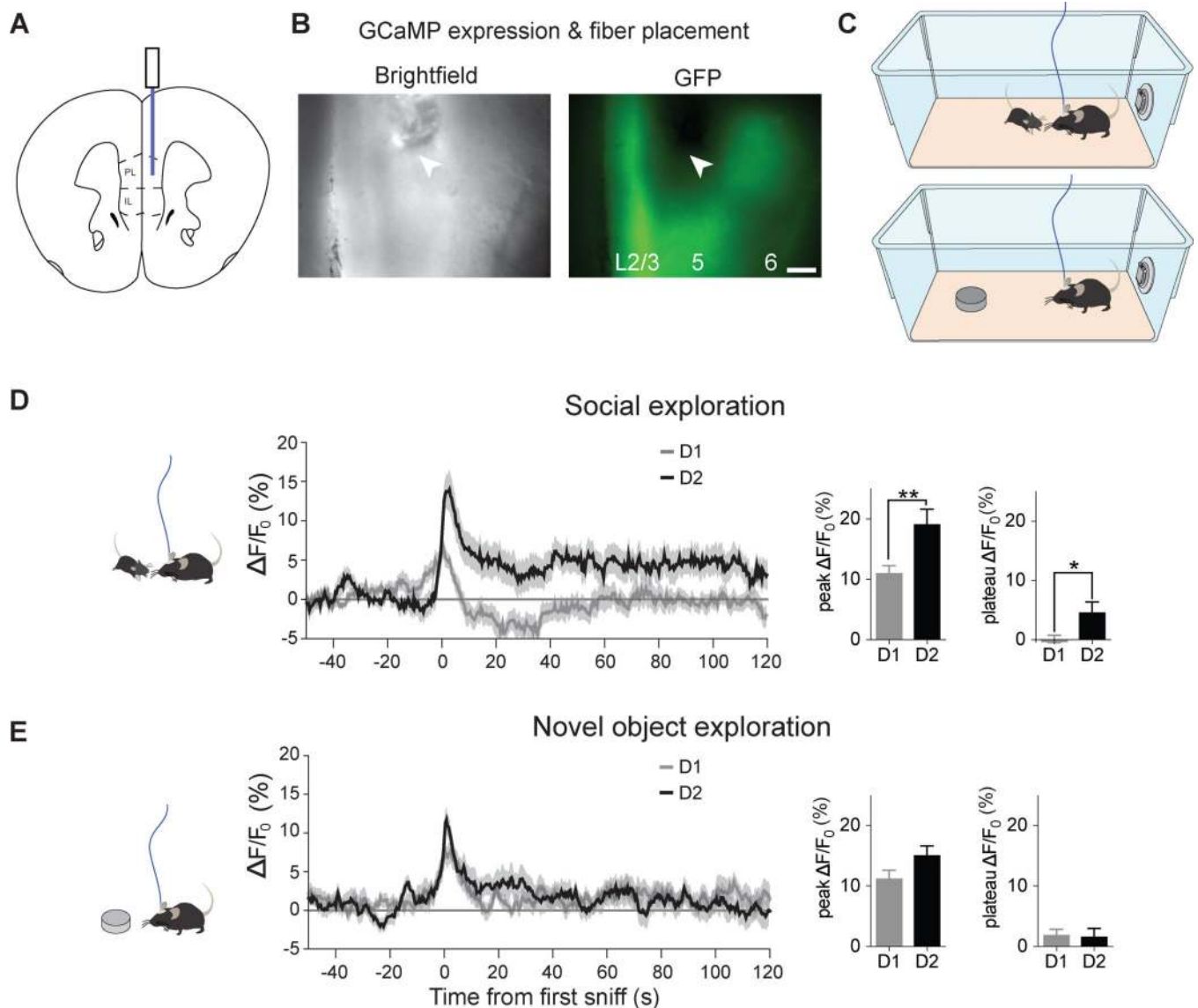
**Figure 3. mPFC D2R+ neurons are persistently activated during social exploration.**
Fluorescence in D2R and D1R expressing cells expressing GCaMP6s during social and novel object exploration in wildtype mice. **A.** Fiber optic implant location for imaging. **B.** Photomicrograph of fiber tip location (arrowheads) relative to Cre-dependent GCaMP6 expression in mPFC. Scale bar = 100 μm. **C.** Home cage social exploration (top) and novel object exploration (bottom) assays. **D.** Left, ΔF/F averaged across mice during social behavior in D1R and D2R-expressing neurons. Right, Quantification of $\Delta F/F_0$ peak and plateau (at +60 seconds averaged over a 20 second window). **E.** $\Delta F/F_0$ averaged across mice during novel object exploration, with quantifications as in D.
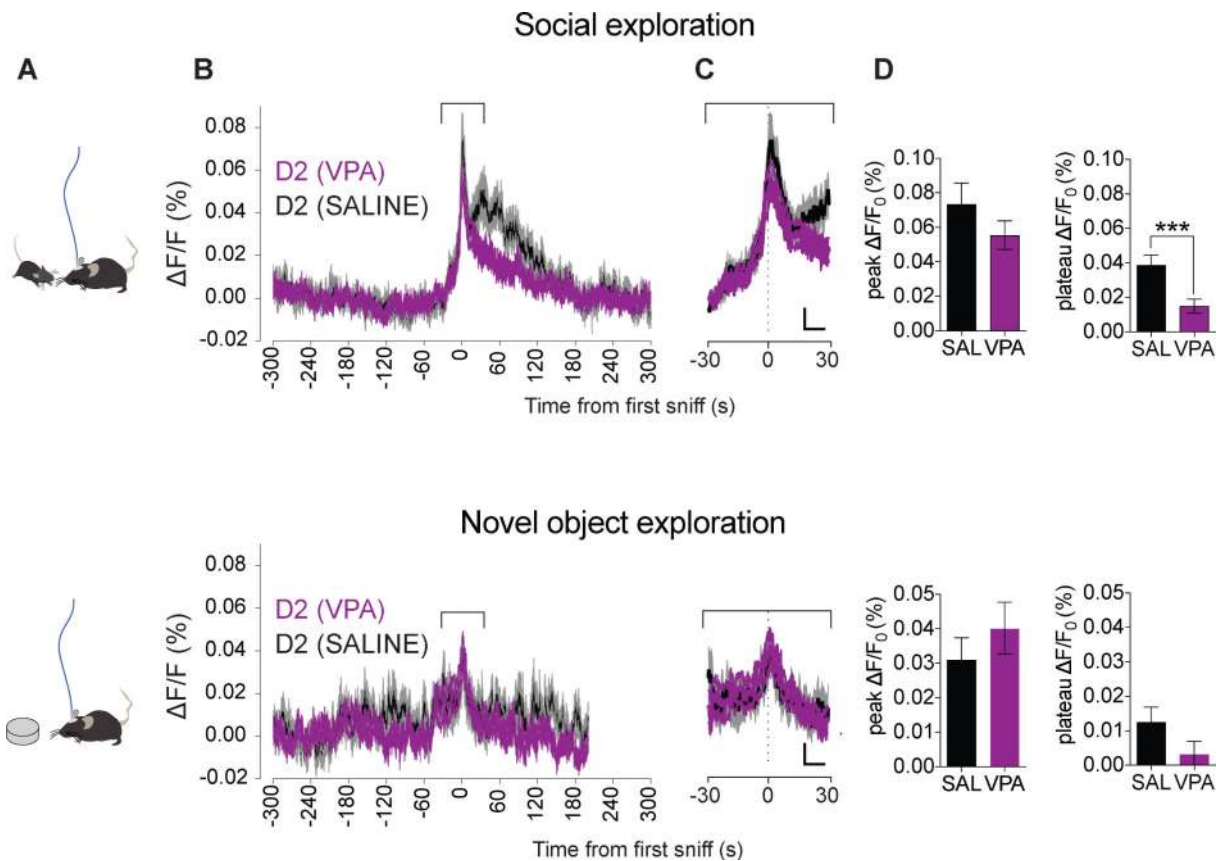
**Figure 4. In VPA mice, mPFC D2R-expressing cells are abnormally activated during social exploration.**

mPFC D2R-GCaMP6f fiber photometry during social (top) or novel object (bottom) exploration in C57Bl/6 VPA mice (purple) or saline controls (black). **A**. Experimental paradigm. **B**. Average GCaMP6f fluorescence during home cage social (top) or novel object (bottom) exploration assay with the first sniff occurring at t = 0 seconds. **C**. Peak fluorescence changes (areas bracketed in **B**) on an expanded time scale. Scale bars = 0.01%, 10 seconds. Dotted line denotes t = 0 s. **D**. Quantification of peak change in fluorescence following initial sniff and the amplitude of the plateau fluorescence (the mean at t = +60 seconds averaged over a 20 second window).
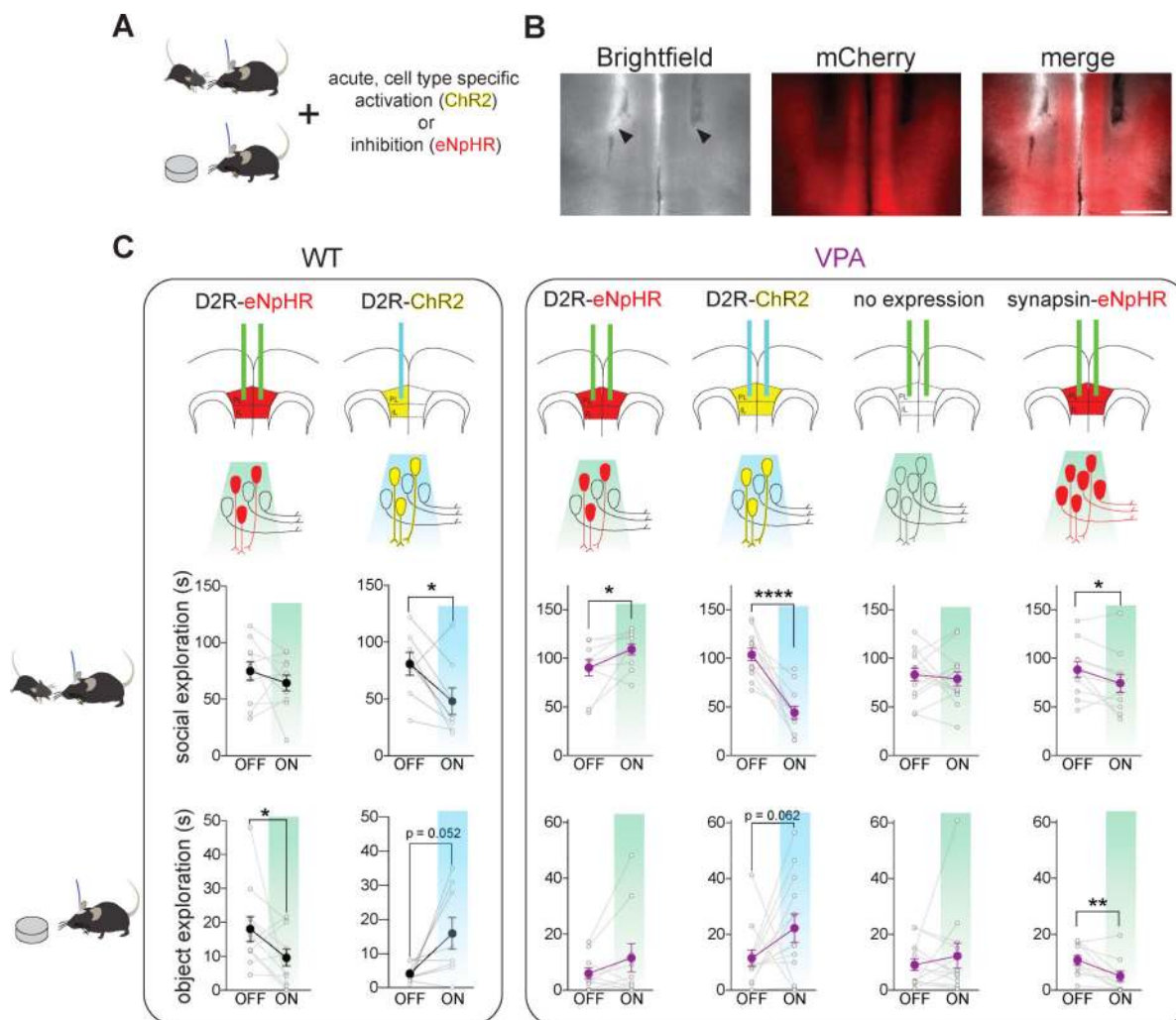
**Figure 5. Acute optogenetic manipulation of D2R-expressing neurons in the mPFC bidirectionally modulates social exploration behavior in VPA mice.**
**A.** Home cage social and novel object exploration assay coupled with acute optogenetic activation (ChR2) or inactivation (eNpHR) of specific neuronal populations. **B.** Photomicrograph of fiber tip locations (arrowheads) within bilateral mPFC relative to expression of the fluorescently tagged opsin (in this case, driven by the synapsin promoter). Scale bar = 500 μm. **C.** In wildtype (left) and VPA (right) mice, acute optogenetic activation (ChR2, yellow) and inactivation (eNpHR, red) of specific mPFC neuron populations during social exploration (top) and novel object exploration (bottom). Each mouse performed the tasks twice, one week apart: once with light ON and once with light OFF. All manipulations were bilateral except for ChR2 stimulation in control mice, which was unilateral. PL, Prelimbic cortex. IL, Infralimbic cortex.